Journal of Materials Chemistry A

RSC Publishing

PAPER

View Article Online
View Journal | View Issue

Cite this: J. Mater. Chem. A, 2013, 1, 11177

Reversible hydrogen storage in $Mg(BH_4)_2$/carbon nanocomposites†

Yigang Yan,‡*[a] Yuen S. Au,‡[b] Daniel Rentsch,[c] Arndt Remhof,[a] Petra E. de Jongh*[b] and Andreas Züttel[a]

Received 7th June 2013
Accepted 18th July 2013

DOI: 10.1039/c3ta12222k

www.rsc.org/MaterialsA

$Mg(BH_4)_2$ exhibits a high hydrogen content of 14.9 wt% and thermodynamic stability in the overall decomposition reaction that corresponds to hydrogen desorption at around room temperature. However, the potential applications in hydrogen storage are restricted by high kinetic barriers. In this study, we show the synthesis of $Mg(BH_4)_2$/carbon nanocomposites by ball milling of MgH_2 nanoparticles supported on carbon aerogel in a B_2H_6/H_2 atmosphere. The nanocomposite exhibits a lower kinetic barrier as compared to bulk $Mg(BH_4)_2$. The temperature for major hydrogen desorption is decreased to 160 °C. Furthermore, re-formation of $Mg(BH_4)_2$ after full dehydrogenation is achieved under mild conditions (200 °C and 80 to 150 bar H_2) in the nanocomposite. This work demonstrates nanoengineering as an effective approach to realize the reversible hydrogen storage of $Mg(BH_4)_2$ under mild conditions.

Introduction

Hydrogen is regarded as a clean energy carrier for the future.[1,2] Achieving safe and efficient hydrogen storage is one of the key technological challenges for the wide use of hydrogen as a fuel. Metal borohydrides, with high gravimetric and volumetric densities of hydrogen, have been extensively investigated for solid state hydrogen storage.[3–5] Among them, magnesium borohydride, *i.e.* $Mg(BH_4)_2$, shows a hydrogen capacity of 14.9 wt% and an attractive enthalpy change of -39 kJ mol^{-1} H_2 in dehydrogenation according to eqn (1).[6–8]

$$Mg(BH_4)_2 \rightarrow MgB_2 + 4H_2 \quad (1)$$

Although the dehydrogenation enthalpy change allows for hydrogen desorption at around room temperature, the major dehydrogenation reaction was observed above 250 °C.[9–11] Rehydrogenation of MgB_2 requires high hydrogen pressure and high temperature (*e.g.* 95 MPa H_2, 400 °C).[12] Numerous studies have revealed that the decomposition reaction (1) occurs in multiple steps involving the formation of Mg–B–H ternary intermediates such as $Mg(B_3H_8)_2$[13] and $MgB_{12}H_{12}$.[11,13–15] The partial decomposition of $Mg(BH_4)_2$ to $Mg(B_3H_8)_2$ can be reversed at 250 °C and 120 bar with a hydrogen release amount of 2.5 wt%. The stable $[B_{12}H_{12}]^{2-}$ species is an unwanted intermediate that reduces the rehydrogenation capacity. The migration of atoms such as Mg and B in the formation process of $[B_{12}H_{12}]^{2-}$ from the reconstruction of $[BH_4]^-$ and the breaking of B–H covalent bonds in $[BH_4]^-$ are considered to result in slow kinetics of the dehydrogenation reaction of $Mg(BH_4)_2$.[15]

An effective approach to accelerate the reaction kinetics is to reduce the particle size and form nanomaterials.[16–19] The faster kinetics is attributed to the shortened diffusion distances and lowered activation energy. By ball milling of MgB_2 in a high pressure hydrogen atmosphere, nanostructured $Mg(BH_4)_2$ was formed with enhanced hydrogen desorption properties.[20,21] Incorporation in a nanoporous scaffold can be used to avoid sintering in the de-/absorption cycles of nanostructured $Mg(BH_4)_2$.[22,23] Infiltration of $Mg(BH_4)_2$ in activated carbon *via* wet impregnation was carried out, resulting in a reduced hydrogen release temperature.[22] The drawbacks of solvent residue and unconfined $Mg(BH_4)_2$ were reported in this method. In recent research, the temperature of hydrogen desorption was reduced to 155 °C by combining nanoconfinement and a Ni catalyst.[23] However, the regeneration of $Mg(BH_4)_2$ under mild conditions from the fully dehydrogenated state has not been reported so far.

Previous studies have demonstrated that solvent free metal borohydrides, such as $LiBH_4$, $Mg(BH_4)_2$, $Ca(BH_4)_2$ and $Y(BH_4)_3$,

[a]EMPA, Swiss Federal Laboratories for Materials Science and Technology, CH 8600 Dübendorf, Switzerland. E-mail: yigang.yan@empa.ch; Fax: +41 58 765 40 22; Tel: +41 58 765 40 82

[b]Inorganic Chemistry and Catalysis, Debye Institute for Nanomaterials Science, Utrecht University, Universiteitsweg 99, 3584 CG Utrecht, The Netherlands. E-mail: p.e.dejongh@uu.nl

[c]EMPA, Swiss Federal Laboratories for Materials Science and Technology, Functional Polymers, 8600 Dübendorf, Switzerland

† Electronic supplementary information (ESI) available: TEM observation and EDX and EELS analysis of MBH-CA and MBH-KS6, thermogravimetry (TG) curves of MBH-CA, MBH-KS6 and bulk $Mg(BH_4)_2$, and cycling property of MBH-CA. See DOI: 10.1039/c3ta12222k

‡ Both authors contributed equally to the work.

can be synthesized *via* reaction between the corresponding metal hydrides and B_2H_6.[24,25] In this study, we applied this method to synthesize nanostructured $Mg(BH_4)_2$. MgH_2 nanoparticles supported on carbon served as precursors and were ball milled in a B_2H_6/H_2 atmosphere to form $Mg(BH_4)_2$ according to eqn (2).

$$MgH_2 + B_2H_6 \rightarrow Mg(BH_4)_2 \quad (2)$$

To investigate the influence of different carbon additives, carbon aerogel (porous structure) and graphite (nonporous structure) were compared.

We observed the formation of nanostructured $Mg(BH_4)_2$, which exhibits a lower temperature for hydrogen release as compared to bulk $Mg(BH_4)_2$. Re-formation of the nanostructured $Mg(BH_4)_2$ also occurred under mild conditions.

Experimental

Carbon aerogel (CA) was synthesized through resorcinol–formaldehyde condensation.[26] Resorcinol (Sigma Aldrich 99%, 8.65 g, 79 mmol), formaldehyde (Fisher Chemical, analytical reagent 37–41%, stabilized by 12% methanol, 12.89 g, 158 mmol) and sodium carbonate (Acros Organics, anhydrous pure, 0.017 g, 0.16 mmol) were dissolved in deionized water. After curing (1 day at room temperature, 1 day at 60 °C and 3 days at 90 °C), the obtained gel was cooled, powdered and subsequently washed with acetone. The gel was pyrolized in a tubular oven at 800 °C for 10 hours in an Ar flow and stored in an Ar purified glovebox (MBraun Labmaster) after cooling to room temperature. Nonporous graphite (KS-6), obtained from Timcal, was pre-treated at 600 °C overnight in an Ar flow. Unless otherwise stated, all sample handlings were carried out in the Argon purified glovebox (O_2 < 0.1 ppm, H_2O < 0.1 ppm) to prevent (hydro-) oxidation.

MgH_2 nanoparticles supported on carbon were prepared *via* melt infiltration.[27] In a typical experiment, 0.9 g of CA or KS-6 was mixed and ground with 0.1 g of MgH_2 in a mortar to obtain a mixture with 10 wt% MgH_2. The mixture was placed in a graphite cup which was inserted in a stainless steel sample holder. The sample was then heated in a tubular oven at 10 °C min^{-1} to 658 °C and dwelled for 24 min under an Ar flow. Hydrogenation of the samples was performed at 80 bar H_2 and 300 °C for 10 h in an autoclave (Parr). The obtained MgH_2 supported on carbon aerogel (CA) and on non-porous graphite (KS-6) are labeled as MH-CA and MH-KS6, respectively. All samples investigated in this study are listed in Table 1.

Table 1 Assignment of the investigated samples. Additionally, a physical mixture of the bulk $Mg(BH_4)_2$ reference with CA in the mass ratio of 1 to 5 is labeled as MBH-CA-PM

Carbon supports	Infiltrated with MgH_2	Ball milled under B_2H_6
Carbon aerogel (CA)	MH-CA	MBH-CA
Non-porous graphite (KS-6)	MH-KS6	MBH-KS6

$LiZn_2(BH_4)_5$, synthesized by ball milling a mixture of $ZnCl_2$ (Sigma-Aldrich, 99.9%) and $LiBH_4$ (Katchem, 95%), was used as a B_2H_6 source releasing B_2H_6 and H_2 above 100 °C according to eqn (3).

$$LiZn_2(BH_4)_5 \rightarrow LiH + 2Zn + 5/2B_2H_6 + 2H_2 \quad (3)$$

500 mg of MH-CA or MH-KS6 was filled in the milling vial connected to the B_2H_6 source. The whole system was purged with hydrogen and evacuated. Subsequently, the diborane source was heated up to 150 °C to fill the system with a B_2H_6/H_2 (5 : 4) atmosphere. After the completion of diborane source desorption, ball milling was carried out for 3 days and the progress of the subsequent reaction was monitored by the pressure change in the milling vial. The samples of MH-CA and MH-KS6 after B_2H_6 treatment were labeled as MBH-CA and MBH-KS6, respectively. Ideally, 10 wt% of MgH_2 in MH-CA could result in 18 wt% of $Mg(BH_4)_2$ (according to eqn (2)) in MBH-CA. In order to compare the effect of different carbon addition methods, a physical mixture of $Mg(BH_4)_2$ with CA, labeled as MBH-CA-PM, was prepared by ball milling of the bulk $Mg(BH_4)_2$ reference (Sigma-Aldrich, 95%) and CA in the mass ratio of 1 to 5 under 10 bar H_2 for 3 days. Also, pure CA was ball milled in B_2H_6/H_2 and H_2 atmosphere, respectively, to investigate the possible reactions between CA with B_2H_6 and H_2.

N_2-physisorption (Micromeritics TriStar 3000) was performed at 77 K for porosity analysis. The total pore volume was obtained at $P/P_0 = 0.997$. The samples were prepared in a capped quartz sample tube in the glovebox and were directly measured. The mesopore size distribution was analyzed with the Barrett–Joyner–Halenda (BJH) method from the adsorption branch of the isotherm with a carbon black thickness equation as reference.

X-ray diffraction (XRD) measurements were performed using a Bruker D8 diffractometer equipped with a Goebel mirror selecting Cu Kα radiation ($\lambda = 1.5418$ Å) and a linear detector system (Vantec). Samples for XRD measurements were filled and sealed in an inert atmosphere into glass capillaries (diameter, 0.7 mm; wall thickness, 0.01 mm).

For transmission electron microscopy (TEM) observation, a small amount of the sample was placed on a 200 mesh Cu grid coated with a carbon polymer film in the glovebox. The sample was exposed for 5 s to air during the insertion of the sample holder into the microscope. Images were recorded with an FEI Tecnai 20F (equipped with a Field Emission Gun) and operated at 200 kV in bright field mode. Elemental analysis was performed with an energy-dispersive X-ray spectrometer (EDX) and an electron energy loss spectrometer (EELS), which were connected to the microscope.

Solid state ^{11}B magic angle spinning nuclear magnetic resonance (MAS NMR) experiments were performed on a Bruker Avance-400 NMR spectrometer using a 4 mm CP-MAS probe. The ^{11}B NMR spectra were recorded at 128.38 MHz at 12 kHz sample rotation applying a Hahn echo pulse sequence to suppress the broad background resonance of boron nitride of the probe. Pulse lengths of 1.5 μs ($\pi/12$ pulse) and 3.0 μs were applied for the excitation and echo pulses, respectively. ^{11}B

NMR chemical shifts are reported in parts per million (ppm) externally referenced to a 1 M $B(OH)_3$ aqueous solution at 19.6 ppm as an external standard sample. The reference sample $K_2B_{12}H_{12}$ was purchased from Katchem.

Thermogravimetric (TG) measurements were carried out by using a magnetic suspension balance (Rubotherm), with a heating rate of 5 °C min^{-1} and an Ar flow of 200 mL min^{-1}. Temperature programmed desorption combined with mass-spectrometry (TPD-MS) (Micromeritics AutoChem II 2920 and Pfeiffer Vacuum OmniStar™) measurements were performed to analyze the decomposition reaction of the samples. Approximately 50 mg of the sample was taken for each measurement. The experiments were carried out in an Ar flow of 25 mL min^{-1} with a temperature ramp of 5 °C min^{-1} up to 500 °C. The masses of B_2H_6 and H_2 were recorded simultaneously over time.

The apparent activation energy (E_a) of hydrogen desorption reaction was determined by using the *Kissinger method* involving the application of eqn (4).[28]

$$\ln\left(\frac{\beta}{T_{max}^{\ 2}}\right) = -\frac{E_a}{RT_{max}} + C \quad (4)$$

Here, β is the heating rate, T_{max} is the peak temperature, R is the gas constant and C is a constant. TPD measurements with different heating rates of 2, 5, 10 and 15 °C min^{-1} were accordingly carried out.

Results

Characterization

CA exhibits a porous structure with a surface area (S_{BET}) of 605 m^2 g^{-1}, a total pore volume of 0.52 cm^3 g^{-1} and an average pore size of 10 nm. After infiltration with Mg, the pore volume of CA is slightly decreased, as shown in Fig. 1. The pore volume is reduced to zero in MBH-CA, indicating that the porous structure of CA was destroyed during the ball milling process.

The XRD patterns of MH-CA and MH-KS6 before and after ball milling in B_2H_6 are shown in Fig. 2. Diffraction peaks of MgH_2 and Mg are observed in samples MH-CA and MH-KS6, indicating the presence of crystalline MgH_2 and Mg on the surfaces of CA and KS6. After ball milling in B_2H_6/H_2, the reflections of Mg and MgH_2 disappear in MBH-CA, while the peak intensities of graphite, MgH_2 and Mg are reduced in MBH-KS6. No observation of new reflections implies that the newly formed compounds by ball milling in a B_2H_6/H_2 atmosphere are amorphous or nanocrystalline. Thereby, NMR spectroscopy is a suitable choice for further phase identification.

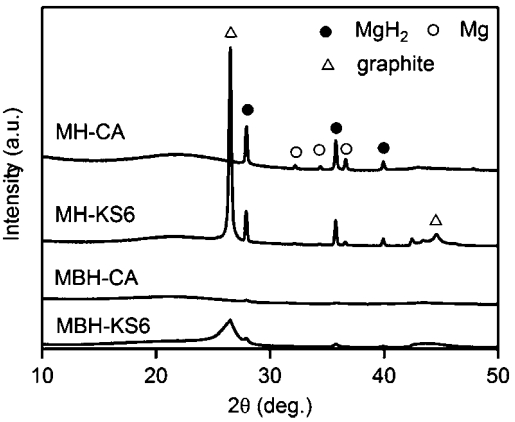

Fig. 2 XRD patterns of carbon supported MgH_2 samples: MH-CA and MH-KS6, and samples after ball milling in B_2H_6/H_2: MBH-CA and MBH-KS6.

The ^{11}B MAS NMR spectrum of MBH-CA in Fig. 3(a) shows two major resonances at −41 and −16 ppm. The resonance at −41 ppm shows the same chemical shift as the reference sample $Mg(BH_4)_2$, indicating the formation of $Mg(BH_4)_2$ in MBH-CA. The signal at −16 ppm belongs to the $[B_{12}H_{12}]^{2-}$ species, which may be formed by a reaction between the newly formed $Mg(BH_4)_2$ compound and B_2H_6. The presence of boron in MBH-CA is also confirmed by EELS as shown in Fig. S1 (ESI†). By integrating the individual peak area in Fig. 3(a), the mass ratio of $Mg(BH_4)_2$ to $MgB_{12}H_{12}$ is estimated to be 1 to 4.5. Considering that the initial amount of Mg is 10 wt% in MH-CA, the amount of $Mg(BH_4)_2$ and $MgB_{12}H_{12}$ in MBH-CA is estimated to be 6 and 27 wt%, respectively, with the remaining 67 wt% being carbon. ^{11}B MAS NMR measurements on MBH-KS6 were

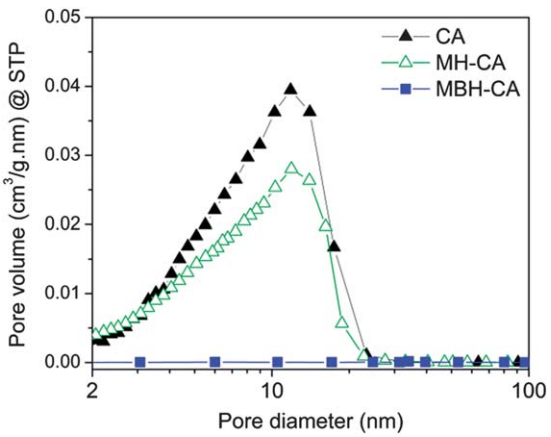

Fig. 1 Pore size distribution of CA, MH-CA and MBH-CA.

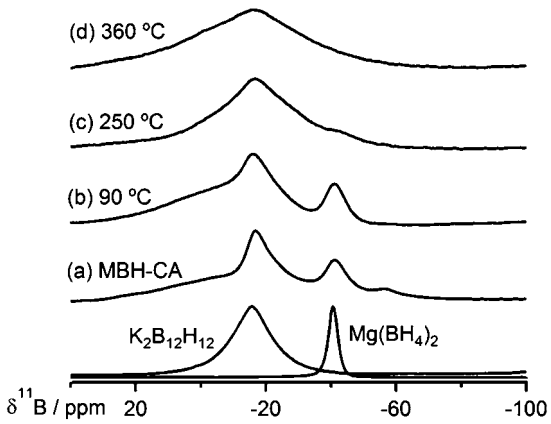

Fig. 3 ^{11}B MAS NMR spectra of (a) as-synthesized MBH-CA, and MBH-CA heated at (b) 90 °C, (c) 250 °C and (d) 360 °C, respectively, compared to the reference samples $K_2B_{12}H_{12}$ and $Mg(BH_4)_2$.

not successful, due to the presence of unpaired electrons in graphite leading to a loss of the NMR signal.[29,30]

Hydrogen desorption properties

The hydrogen desorption behaviors of MBH-CA, MBH-KS6 and two reference samples were examined by TPD and MS. In Fig. 4(a), the desorption of the bulk $Mg(BH_4)_2$ reference starts from 250 °C. The three desorption peaks present within the temperature range of 270 to 400 °C apparently correspond to three decomposition steps.[9] Only traces of B_2H_6 are detected by MS, as shown in Fig. 4(b). MBH-CA-PM shows a broad desorption peak within the same temperature region as bulk $Mg(BH_4)_2$.

The hydrogen desorption behaviors of MBH-CA and MBH-KS6 (Fig. 4(a)) are quite different from those of the reference samples. The desorption of MBH-CA starts around 100 °C, approximately 150 °C lower than that of bulk $Mg(BH_4)_2$, which is in good agreement with TG results in Fig. S2 (ESI†). The first desorption step of MBH-CA occurs at 160 °C and the second step at 335 °C. The simultaneous MS measurement in Fig. 4(b) reveals that the gas release in the TPD measurement is mainly due to the release of H_2 and only a slight amount of B_2H_6 is detected. The first desorption peak of MBH-KS6 is also found at 160 °C (Fig. 4(a)). In addition, two other desorption peaks are observed at 285 and 336 °C, within a similar temperature range as the decomposition of bulk $Mg(BH_4)_2$. In summary, $Mg(BH_4)_2$ supported on different carbon matrixes shows different desorption behaviors.

Note that the release of B_2H_6 occurs at a lower temperature (below 100 °C) than that of H_2 for both MBH-CA and MBH-KS6 (shown in Fig. 4(b)). The released B_2H_6 is possibly attributed to physisorption or trapping of B_2H_6 on carbon during the ball milling process. To verify this hypothesis, pure CA was ball milled under a B_2H_6/H_2 and a pure H_2 atmosphere, respectively, and examined by MS. In Fig. 5, MS data of MBH-CA and milled CA are compared. It is clearly observed that H_2 is also desorbed from the ball milled CA in B_2H_6/H_2 but without distinct peaks, and the H_2 release profile of CA appears to follow the baseline of that of MBH-CA. Defects could be created in the carbon structure during the ball milling process, possibly leading to the formation of C–B–H chemical bonds. Ball milling of CA in the pure H_2 atmosphere only results in traces of hydrogen release above 350 °C, possibly due to the formation of stable C–H bonds. Therefore, the hydrogen desorption peaks of MBH-CA at 160 and 335 °C (Fig. 5) can be ascribed to the decomposition of $Mg(BH_4)_2$. The ball milled CA under B_2H_6/H_2 also shows a different B_2H_6 release behavior compared to MBH-CA, *i.e.* two B_2H_6 peaks at 120 and 250 °C, respectively, and the B_2H_6 release at 120 °C is very limited. This indicates that the B_2H_6 release of MBH-CA mainly originates from $Mg(BH_4)_2$.

To clarify the evolution of the boron species in MBH-CA during the decomposition process, MBH-CA was decomposed at different temperatures and examined by ^{11}B MAS NMR. As shown in Fig. 3, the resonance assigned to $[BH_4]^-$ is present at

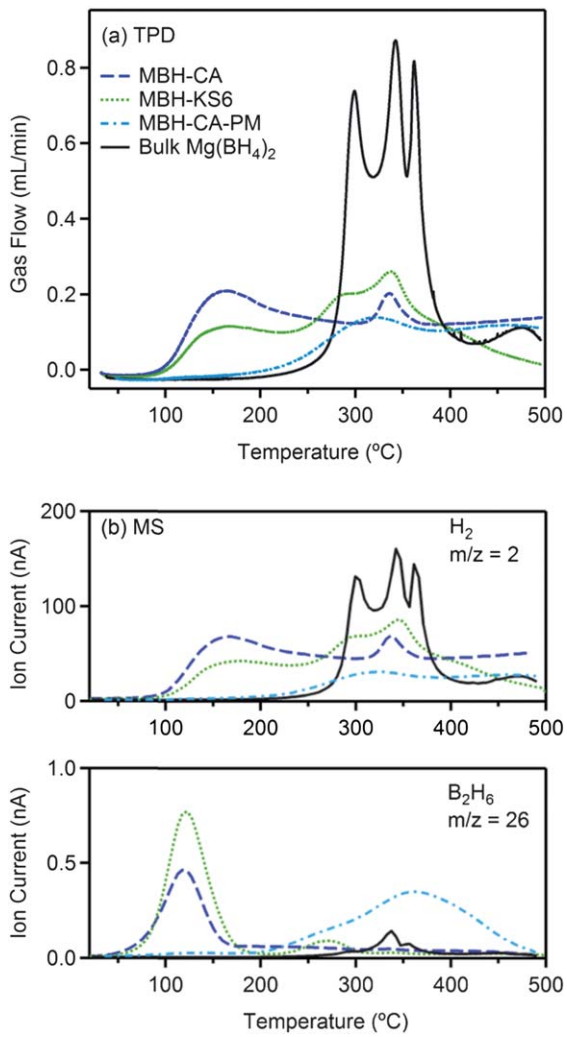

Fig. 4 (a) TPD spectra and (b) MS profiles of MBH-CA, MBH-KS6, MBH-CA-PM and bulk $Mg(BH_4)_2$.

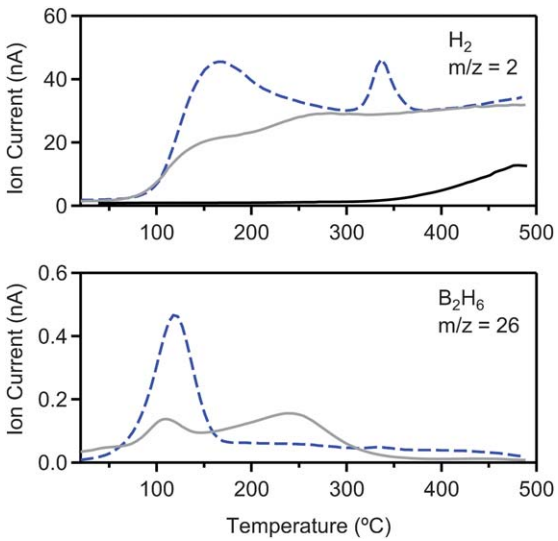

Fig. 5 MS profiles of MBH-CA (blue, dashed line), and CA ball milled in a B_2H_6/H_2 (gray line) and CA ball milled in a H_2 atmosphere (black line) for 3 days.

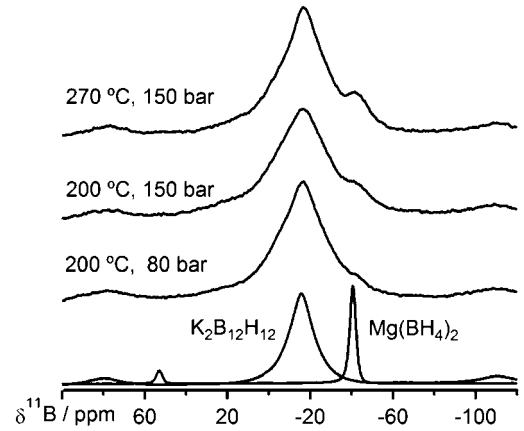

Fig. 6 ^{11}B MAS NMR spectra of MBH-CA rehydrogenated at 200 °C and 270 °C, respectively.

90 °C and disappears at 250 °C. The resonance centered at −16 ppm assigned to the $[B_{12}H_{12}]^{2-}$ species is present up to 360 °C, indicating the high stability of $MgB_{12}H_{12}$.

Reversibility

According to the results in Fig. 4 and 5, the hydrogen desorption from $Mg(BH_4)_2$ in MBH-CA shows apparently two steps and is completed below 360 °C. To examine the reversibility of $Mg(BH_4)_2$ supported on CA, the sample of MBH-CA was decomposed at 360 °C and rehydrogenated under 150 bar H_2 at 200 or 270 °C and under 80 bar at 200 °C, respectively. The ^{11}B MAS NMR spectra of the rehydrogenated samples are shown in Fig. 6. The re-formation of $Mg(BH_4)_2$ is observed at both 200 and 270 °C under 150 bar. By carrying out rehydrogenation at a lower H_2 pressure of 80 bar at 200 °C, traces of $Mg(BH_4)_2$ were formed as well. In contrast, the rehydrogenation of bulk $Mg(BH_4)_2$ requires higher pressures (*e.g.* 900 to 950 bar of H_2) and higher temperatures (*e.g.* 390 to 400 °C).[12,29]

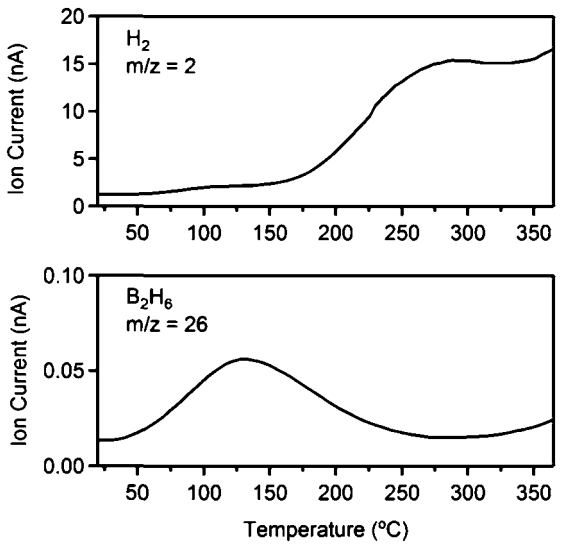

Fig. 7 MS profiles of MBH-CA rehydrogenated at 270 °C and 150 bar for 20 h.

Fig. 7 shows the hydrogen desorption of the sample rehydrogenated at 270 °C. In the 2nd cycle, less hydrogen is released and the hydrogen desorption temperature is increased to 200 °C, indicating the deterioration of the H_2 desorption properties. In addition, desorption of B_2H_6 was also observed at 120 °C, similar to that of the as-synthesized sample (Fig. 4).

Discussion

$Mg(BH_4)_2$/carbon nanocomposites were successfully synthesized by ball milling of MgH_2 nanoparticles supported on carbon aerogel in a B_2H_6/H_2 atmosphere at room temperature, exhibiting a lower desorption temperature and reversibility under milder conditions as compared to bulk $Mg(BH_4)_2$.

The reduced hydrogen desorption temperature of MBH-CA is attributed to the formation of nanostructured $Mg(BH_4)_2$. Reducing the particle size of hydrides to nanoscale improves the H_2 sorption kinetics and decreases the reaction temperature.[30–34] The improvement in kinetics by a "nanosize effect" arises from the lowered activation barrier and the shortened diffusion distance of atoms in the nanoscale structures. The activation energies (E_a) of the first hydrogen desorption step of MBH-CA and bulk $Mg(BH_4)_2$ are compared in Fig. 8. In the sample MBH-CA, the nanostructured $Mg(BH_4)_2$ shows a markedly lowered E_a of 102 ± 6 kJ mol^{-1}, compared to 340 ± 11 kJ mol^{-1} for bulk $Mg(BH_4)_2$.

Possibly due to the accelerated kinetics, the hydrogen desorption process of $Mg(BH_4)_2$ is altered from an apparently 3-step reaction for the bulk $Mg(BH_4)_2$ to a 2-step reaction for MBH-CA. A catalytic effect of the carbon matrix was not found for improving the kinetics in MBH-CA. When carbon aerogel was introduced into bulk $Mg(BH_4)_2$ in the mass ratio of 5 to 1 by ball milling, the hydrogen desorption temperature was only slightly reduced, as observed in the sample MBH-CA-PM (shown in Fig. 4).

Since the porous structure of carbon aerogel in MBH-CA was destroyed during the ball milling process, a possible effect due to nanoconfinement cannot be determined. The

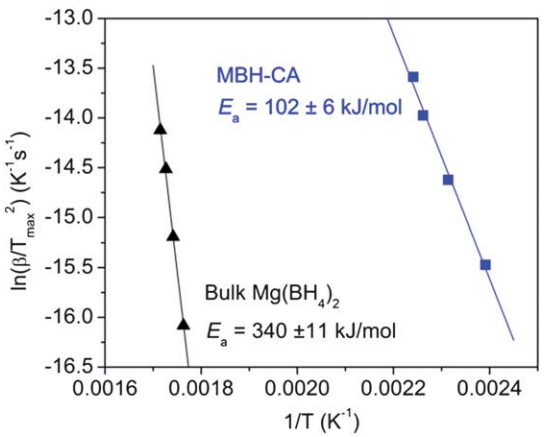

Fig. 8 Kissinger plot of the first hydrogen desorption step for MBH-CA and bulk $Mg(BH_4)_2$.

newly formed $Mg(BH_4)_2$ is very likely dispersed homogeneously on the non-porous carbon matrix with this synthesis method (see Fig. S1a†). In this sense, ball milling of MgH_2 supported on nonporous graphite in B_2H_6/H_2 could also lead to the formation of nanostructured $Mg(BH_4)_2$, which is responsible for the hydrogen desorption reaction occurring at 160 °C in Fig. 4. The hydrogen desorption reactions at 285 and 336 °C that occur within a temperature range similar to the desorption of bulk $Mg(BH_4)_2$ (Fig. 4(b)) imply the existence of bulk $Mg(BH_4)_2$ in MBH-KS6. This could be related to the observation of some crystalline MgH_2 in the XRD pattern of MBH-KS6 (Fig. 2).

Fig. 9 summarizes schematically the images of bulk $Mg(BH_4)_2$, MBH-CA-PM, MBH-KS6 and MBH-CA, and their temperature ranges for hydrogen desorption are compared. Apparently, the smaller the particle size, the lower the desorption temperature; this tendency implies a relationship between particle size and hydrogen sorption performance of $Mg(BH_4)_2$, similar to the observations in other hydrides such as $LiBH_4$[31,35] and MgH_2.[36] The argument of a nanosize effect may also apply to the improved rehydrogenation performance of MBH-CA. The rehydrogenation reaction of bulk $Mg(BH_4)_2$ from MgB_2 according to eqn (1) needs a high temperature (*e.g.* 400 °C) due to the large kinetic barrier.[12] According to the thermodynamic properties of $Mg(BH_4)_2$,[6-8] a high hydrogen pressure over 660 bar is required for rehydrogenation at 400 °C, as displayed in Fig. 10. Following the van't Hoff plot of eqn (1), partial reformation of $Mg(BH_4)_2$ was achieved under milder conditions (200 to 270 °C under 150 bar H_2) for the nanostructured sample. By applying a lower H_2 pressure of 80 bar at 200 °C, less $Mg(BH_4)_2$ was formed (shown in Fig. 6) due to the lower driving force.

About 30% of hydrogen can be re-absorbed in the second cycle at 270 °C and 150 bar, as shown in Fig. S3.† The decay in H_2 desorption properties could be attributed to sintering of nanoparticles during the desorption and reabsorption processes, since the pore structure of the carbon matrix in MBH-CA was destroyed by ball milling. However, it is difficult to observe the change in morphology of nanoparticles before (Fig. S1†) and after recycling (Fig. S4†) by TEM, due to the low contrast between carbon, boron and Mg. Despite that, the B_2H_6 desorption in the 2nd cycle (Fig. 7) remains at the same temperature compared to the as-synthesized MBH-CA (Fig. 4(b)), indicating the formation of $Mg(BH_4)_2$ nanoparticles after rehydrogenation.

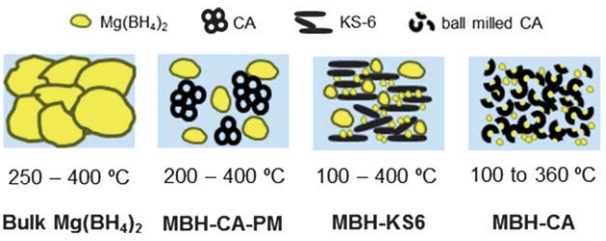

Fig. 9 Schematic images of bulk $Mg(BH_4)_2$, MBH-CA-PM, MBH-KS6 and MBH-CA, with corresponding temperature ranges for hydrogen desorption.

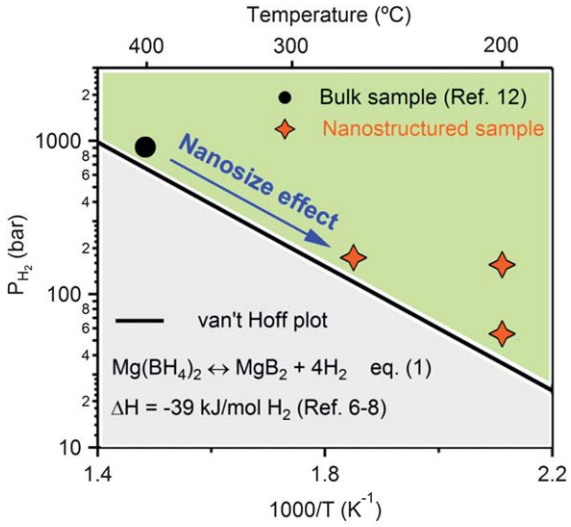

Fig. 10 van't Hoff plot of reaction $Mg(BH_4)_2 \leftrightarrow MgB_2 + 4H_2$ and comparison of rehydrogenation conditions (*e.g.* temperature and hydrogen pressure) of bulk $Mg(BH_4)_2$ (circle)[12] and nanostructured $Mg(BH_4)_2$ (stars). The reduction in pressure and temperature for rehydrogenation reaction is attributed to a nanosize effect.

Conclusions

We present the synthesis of $Mg(BH_4)_2$/carbon composites by ball milling of MgH_2 supported on the carbon matrix in a B_2H_6/H_2 atmosphere. When carbon aerogel (average pore size of 10 nm) was taken as the carbon support, a $Mg(BH_4)_2$/carbon nanocomposite (MBH-CA) was obtained. ^{11}B MAS NMR measurements confirmed the formation of $Mg(BH_4)_2$. MBH-CA exhibits a markedly reduced activation energy of 102 ± 6 kJ mol^{-1} compared to 340 ± 11 kJ mol^{-1} for bulk $Mg(BH_4)_2$, and a lowered temperature (160 °C) for the major hydrogen desorption. When nonporous graphite was used as the carbon support, the formed $Mg(BH_4)_2$/carbon composite (MBH-KS6) also shows a hydrogen desorption peak at 160 °C, indicating the presence of nanostructured $Mg(BH_4)_2$. In addition, the desorption reactions occurring at 285 and 336 °C within a similar temperature range as the decomposition of bulk $Mg(BH_4)_2$ imply the presence of bulk $Mg(BH_4)_2$ in MBH-KS6 as well.

Re-formation of $Mg(BH_4)_2$ from dehydrogenated MBH-CA was achieved under mild conditions (200 °C and 80 to 150 bar H_2). The deterioration in hydrogen desorption performance during the 2nd sorption cycle is possibly due to sintering of nanoparticles. Therefore, maintenance of the nanostructures is considered to be important for the reversible hydrogen sorption performance of $Mg(BH_4)_2$ under mild conditions.

Acknowledgements

The authors would like to acknowledge the financial support granted by Switzerland through the Swiss Contribution to the enlarged European Union, a grant from the Dutch organization for scientific research (NWO Vidi (016.072.316)), and by the Korean Research Council. Part of this work was supported by

COST Action MP1103 "Nanostructured materials for solid-state hydrogen storage". We thank J.D. Meeldijk for acquiring the TEM images and J. Geus for his advice on the EELS measurements. We are grateful to Timcal for providing us with the carbon support materials.

Notes and references

1 L. Schlapbach, *Nature*, 2009, **460**, 809–811.
2 A. Zuttel, A. Remhof, A. Borgschulte and O. Friedrichs, *Philos. Trans. R. Soc., A*, 2010, **368**, 3329–3342.
3 J. Graetz, *Chem. Soc. Rev.*, 2009, **38**, 73–82.
4 J. Yang, A. Sudik, C. Wolverton and D. J. Siegel, *Chem. Soc. Rev.*, 2010, **39**, 656–675.
5 H. W. Li, Y. G. Yan, S. Orimo, A. Zuttel and C. M. Jensen, *Energies*, 2011, **4**, 185–214.
6 M. J. van Setten, G. A. de Wijs, M. Fichtner and G. Brocks, *Chem. Mater.*, 2008, **20**, 4952–4956.
7 V. Ozolins, E. H. Majzoub and C. Wolverton, *J. Am. Chem. Soc.*, 2009, **131**, 230–237.
8 Y. Yan, H. W. Li, Y. Nakamori, N. Ohba, K. Miwa, S. Towata and S. Orimo, *Mater. Trans.*, 2008, **49**, 2751–2752.
9 H. W. Li, K. Kikuchi, Y. Nakamori, N. Ohba, K. Miwa, S. Towata and S. Orimo, *Acta Mater.*, 2008, **56**, 1342–1347.
10 N. Hanada, K. Chlopek, C. Frommen, W. Lohstroh and M. Fichtner, *J. Mater. Chem.*, 2008, **18**, 2611–2614.
11 G. L. Soloveichik, Y. Gao, J. Rijssenbeek, M. Andrus, S. Kniajanski, R. C. Bowman, S. J. Hwan and J. C. Zhao, *Int. J. Hydrogen Energy*, 2009, **34**, 916–928.
12 G. Severa, E. Ronnebro and C. M. Jensen, *Chem. Commun.*, 2010, **46**, 421–423.
13 M. Chong, A. Karkamkar, T. Autrey, S. Orimo, S. Jalisatgi and C. M. Jensen, *Chem. Commun.*, 2011, **47**, 1330–1332.
14 S. J. Hwang, R. C. Bowman, J. W. Reiter, J. Rijssenbeek, G. L. Soloveichik, J. C. Zhao, H. Kabbour and C. C. Ahn, *J. Phys. Chem. C*, 2008, **112**, 3164–3169.
15 H. W. Li, K. Miwa, N. Ohba, T. Fujita, T. Sato, Y. Yan, S. Towata, M. W. Chen and S. Orimo, *Nanotechnology*, 2009, **20**, 204013.
16 X. B. Chen, C. Li, M. Gratzel, R. Kostecki and S. S. Mao, *Chem. Soc. Rev.*, 2012, **41**, 7909–7937.
17 M. Fichtner, *Adv. Eng. Mater.*, 2005, **7**, 443–455.
18 J. J. Vajo, *Curr. Opin. Solid State Mater. Sci.*, 2011, **15**, 52–61.
19 P. Adelhelm and P. E. de Jongh, *J. Mater. Chem.*, 2011, **21**, 2417–2427.
20 S. Gupta, I. Z. Hlova, T. Kobayashi, R. V. Denys, F. Chen, I. Y. Zavaliy, M. Pruski and V. K. Pecharsky, *Chem. Commun.*, 2013, **49**, 828–830.
21 C. Pistidda, S. Garroni, F. Dolci, E. G. Bardaji, A. Khandelwal, P. Nolis, M. Dornheim, R. Gosalawit, T. Jensen, Y. Cerenius, S. Surinach, M. D. Baro, W. Lohstroh and M. Fichtner, *J. Alloys Compd.*, 2010, **508**, 212–215.
22 M. Fichtner, Z. Zhao-Karger, J. J. Hu, A. Roth and P. Weidler, *Nanotechnology*, 2009, **20**, 204029.
23 M. A. Wahab, Y. Jia, D. J. Yang, H. J. Zhao and X. D. Yao, *J. Mater. Chem. A*, 2013, **1**, 3471–3478.
24 A. Remhof, A. Borgschulte, O. Friedrichs, P. Mauron, Y. Yan and A. Zuttel, *Scr. Mater.*, 2012, **66**, 280–283.
25 O. Friedrichs, A. Remhof, A. Borgschulte, F. Buchter, S. I. Orimo and A. Zuttel, *Phys. Chem. Chem. Phys.*, 2010, **12**, 10919–10922.
26 R. W. Pekala and F. M. Kong, *J. Phys.*, 1989, **50**, C433–C440.
27 P. E. de Jongh, R. W. P. Wagemans, T. M. Eggenhuisen, B. S. Dauvillier, P. B. Radstake, J. D. Meeldijk, J. W. Geus and K. P. de Jong, *Chem. Mater.*, 2007, **19**, 6052–6057.
28 H. E. Kissinger, *Anal. Chem.*, 1957, **29**, 1702–1706.
29 R. J. Newhouse, V. Stavila, S. J. Hwang, L. E. Klebanoff and J. Z. Zhang, *J. Phys. Chem. C*, 2010, **114**, 5224–5232.
30 A. Gutowska, L. Y. Li, Y. S. Shin, C. M. M. Wang, X. H. S. Li, J. C. Linehan, R. S. Smith, B. D. Kay, B. Schmid, W. Shaw, M. Gutowski and T. Autrey, *Angew. Chem., Int. Ed.*, 2005, **44**, 3578–3582.
31 A. F. Gross, J. J. Vajo, S. L. Van Atta and G. L. Olson, *J. Phys. Chem. C*, 2008, **112**, 5651–5657.
32 Y. F. Liu, K. Zhong, K. Luo, M. X. Gao, H. G. Pan and Q. D. Wang, *J. Am. Chem. Soc.*, 2009, **131**, 1862–1870.
33 P. Ngene, M. van Zwienen and P. E. de Jongh, *Chem. Commun.*, 2010, **46**, 8201–8203.
34 T. Mueller and G. Ceder, *ACS Nano*, 2010, **4**, 5647–5656.
35 X. F. Liu, D. Peaslee, C. Z. Jost, T. F. Baumann and E. H. Majzoub, *Chem. Mater.*, 2011, **23**, 1331–1336.
36 M. Paskevicius, D. A. Sheppard and C. E. Buckley, *J. Am. Chem. Soc.*, 2010, **132**, 5077–5083.